Characterisation of aqueous interfaces with different hydrophobicities by molecular dynamics

Buuren, Aldert R. van; Marrink, Siewert-Jan; Berendsen, Herman J.C.

Published in:
Colloids and Surfaces A-Physicochemical and Engineering Aspects

DOI:
10.1016/0927-7757(95)03227-5

Publication date:
1995

ELSEVIER

Colloids and Surfaces
A: Physicochemical and Engineering Aspects 102 (1995) 143–157

COLLOIDS AND SURFACES A

Characterisation of aqueous interfaces with different hydrophobicities by molecular dynamics

Aldert R. van Buuren, Siewert-Jan Marrink, Herman J.C. Berendsen *

BIOSON Research Institute and Laboratory of Biophysical Chemistry, University of Groningen, Nijenborgh 4, 9747 AG Groningen, The Netherlands

Received 7 November 1994; accepted 12 April 1995

Abstract

We have analyzed various surface properties for a number of simulated surfaces with water as one of the bulk phases. The structural ordering of water and of the lipid phase have also been considered. Although the simulations concern widely varying hydrophobic and hydrophilic components and cover a range of temperatures, the various surface structures show very similar properties. The roughness of the interfaces varies between 0.5 nm for liquid interfaces and 1 nm for interfaces containing surfactant molecules. The mobility that accounts for the most important movements at the simulated interfaces occur on a 10 ps time scale. Apart from the — generally dominant — water polarization in response to primary charges and dipoles, water exhibits a slight preferential orientation with its dipole directed outwards from the water phase.

Keywords: Aqueous interfaces; Hydrophobicity; Molecular dynamics

1. Introduction

Computational chemistry has enjoyed a rapid development during recent decades and computer simulation is now generally accepted as a complementary tool to experimental methods [1]. If the procedure is properly validated, atomic details that cannot be obtained experimentally can be accessed with computer simulations. In this paper computer simulations using molecular dynamics (MD) are described. In MD the classical equations of motion of the system are solved as a function of time. The time averages of the trajectory give structural properties and most thermodynamic properties (but not all, like entropy and free energy); time-dependent correlations yield non-equilibrium and transport properties. It is not our intention to go into detail on the simulation technique: for more detailed information we refer the reader to the book of Allen and Tildesley [2]. For a general review on MD methodology, applications and perspectives in chemistry see Ref. [3].

Aqueous interfaces play an important role in "real life" because many important processes take place at these interfaces. Scientists in different disciplines are trying to understand the structure and function of aqueous interfaces. Recent computer simulations of aqueous interfaces, have revealed a considerable amount of information on a structural and molecular level, for example water/liquid interfaces [4–8], water/amphiphile/liquid or vacuum interfaces [9–11] and water/amphiphile bilayer interfaces [12–20].

The molecular structure of aqueous interfaces

* Corresponding author.

SSDI 0927-7757(95)03227-4

has already been nicely reviewed by Pohorille and Wilson [21], but in our opinion there are still some properties that need to be discussed. For this purpose we will use the results of four simulations that were performed in our laboratory ranging from hydrophobic (decane/water and diglyceride/water) to hydrophilic (phospholipid membrane and surfactant/decane/water) interfaces. Subjects of special discussion are the width of the interface and its fractal character, free volume distribution, the electrostatic potential, mobility and ordering of water and lipid molecules at the various aqueous interfaces. We compare available experimental data with simulations. We shall consider MD simulations with full atomic detail, thus excluding simulations on model systems without an explicit solvent or with simplified potentials [22–27].

2. Methods

2.1. Method of simulation

The energy of a molecular system is described by simple potential energy functions which include stretch, bend, torsional, Lennard-Jones, and electrostatic interaction. We applied GROMOS force field [28], with the latest modifications for the carbon-oxygen interaction [5]. Atomic detail is used except for hydrogen atoms bound to carbon atoms, which we treated as united atoms and no special hydrogen-bond term is included. The water is modeled as a simple point charge (SPC) [29]. For the diglyceride simulation we used the GROMACS package [30], a parallel GROMOS-like implementation. More details about the simulation method plus a complete description of the force field can be found in the publications as listed in Table 1.

2.2. Models

The four models we compare in this paper are a dipalmitoylphosphatidylcholine (DPPC) membrane, a decyl-β-glucoside monolayer (GLCB) (at the decane/water interface), decane (DEC)/water and dilauroyl-*sn*-glycerol (GLYC)/water. The simulation parameters are listed in Table 1. A depiction of the compounds is presented in Fig. 1. One of the main differences between these molecules is the head group: a bulky choline (for DPPC); a glucose group (for GLCB), a small glycerol backbone (for GLYC) and no head group at all (for DEC). The tails differ in length as well as in

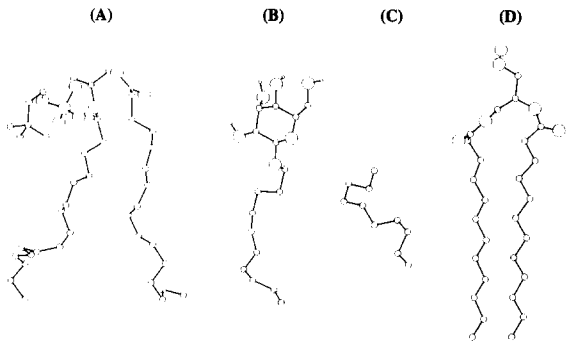

Fig. 1. Schematics of the four molecules used: (A), DPPC; (B), GLCB; (C), DEC; (D), GLYC.

Table 1
Simulation parameters of the four different models

System	Lipids	Water	Atoms	Box (nm)[a]	T (K)	Time (ps)
DPPC[b,c] [13–15]	64	1867	7700	4.4 × 4.5 × 7.0	350	80
GLCB[d] [9]	72	1548	8686	4.2 × 4.2 × 9.0	315	250
DEC[c] [5]	50	389	1667	2.5 × 2.5 × 4.6	315	500
GLYC[c] [6]	100	1419	7557	5.3 × 3.7 × 6.3	300	2000

[a] Box length in x-, y-, z-direction.
[b] The number of water molecules is variable as described in Ref. [14].
[c] At constant pressure and temperature.
[d] At constant volume and temperature.

number, ranging from a single C_{10} alkyl tail to a double (saturated) C_{16} alkyl tail.

3. Results and discussion

3.1. The interface

Density profiles

In Fig. 2 the density profiles of the different interfaces are plotted. From these profiles it is clear that DPPC and GLCB have a much broader interface because they have big polar head groups. As a result of these head groups, the water density drops much less rapidly for DPPC and GLCB than for the other two systems. GLYC has a slightly broader interface than DEC due to oxygen atoms in the glycerol linkage which increases the hydrophilic character of the interface. Therefore, the interface is the sharpest for DEC.

When comparing the widths of these interfaces with those which appear in the literature, and defining the width of the interface as the distance over which the water density drops from 90 to 10%, we can conclude that the interfacial width for hydrophobic surfaces differs from hydrophilic surfaces. For hydrophobic surfaces the interfacial width is around 0.5 nm and for hydrophilic surfaces around 1.0 nm.

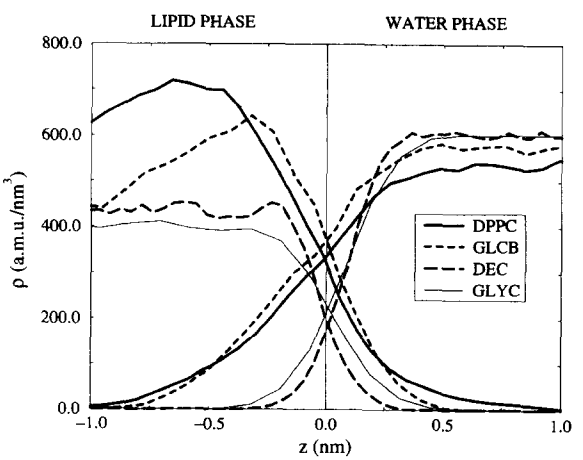

Fig. 2. Density profiles against z-position in the box. The interface is arbitrarily defined at the point where the water density equals the lipid density and all the plots have been translated from that point to zero.

From the plots in Fig. 2 it is not clear that the water molecules penetrate the hydrophobic core, whcih they in fact do. The residence time however, is short, up to several picoseconds. Most of the simulations reported so far, observed minimal water penetration into the hydrophobic regions. When looking closer at the interface by means of a video animation [31,32], we clearly see that water molecules occasionally penetrate into the hydrophobic region and remain there for some time.

Particle-accessible surface

At the microscopic level, the neighbouring atoms can be connected by small segments of a plane or some other kind of smooth surface to describe the topography of the surface. This will clearly give a different picture than when looking on a macroscopic level, where all simulated surfaces look smooth since long range fluctuations are not allowed due to periodic boundary conditions.

A measure of the roughness of interfaces is the van der Waals surface as measured by a probe particle with radius R. The degree of irregularity of this surface can be described by the fractal dimension (d_f), with $2 \leqslant d_f \leqslant 3$. As the surfaces become more irregular, the fractal dimension increases, ranging from $d_f = 2$ for a smooth surface, to $d_f \leqslant 3$ [33,34]. From the relation

$$\log (A/A_0) \propto \log (R^{2-d_f}) \tag{1}$$

one can calculate d_f where A is the van der Waals surface area, A_0 is the lateral area of the interface and R is the probe radius. So d_f is a measure of irregularity by comparison with a fixed shape, however the result does not depend on the chosen standard [33]. In Fig. 3 the accessible surface with respect to probe size is presented. For a small probe it is clear that the surface of DPPC and GLCB are much rougher than for GLYC and DEC. DPPC is still very rough for probes of medium size. The radius of a water molecule is around 0.15 nm.

The term fractal dimension for d_f is not really appropriate because the log–log plots are not linear over a significant range of probe radii. Nevertheless, the value of d_f as a function of probe

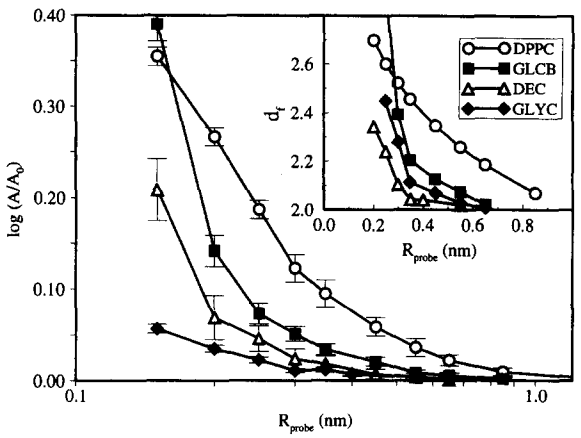

Fig. 3. Ratio of the surface area and accessible surface against probe size. Insert: fractal dimension.

radius gives a clear indication of the surface roughness as seen by the probe particle (inset of Fig. 3). For probes with diameters between 0.2 and 0.4 nm, the surface proves to be very rough, with a fractal dimension around 2.5. For a larger probe size there is a cross-over to a lower fractal dimension, which is due to the self-affine nature of the surface (i.e. different scaling behaviour in the lateral vs. perpendicular direction). In the limit of infinite-sized probe particles, the surface will behave like a flat sheet, with (fractal) dimension 2. At the small probe size limit, one sees that the fractal dimension increases. This can be attributed to the porous nature of the membrane on scales smaller than 0.2 nm. For GLCB, DEC and GLYC, d_f decreases rapidly to 2 (flat surface) when the probe size is increased, whereas for DPPC this effect is not as pronounced. DEC and GLYC show the least rough surface, being "flat" beyond $R = 0.4$ nm.

In Figs. 4, 5, 6 and 7 the van der Waals surfaces are plotted to give an idea of the difference in roughness between these interfaces when using increasing probe size. The different probe sizes used are related to the radius of a choline group (about 0.3 nm), a disaccharide (around 0.7 nm), and a small protein (around 1.5 nm). From these figures it is also clear that all the surfaces look more or less the same for large probes, whereas for small probes, the hydrophilic surfaces are much rougher. The plot with $R = 0.25$ nm for DPPC and

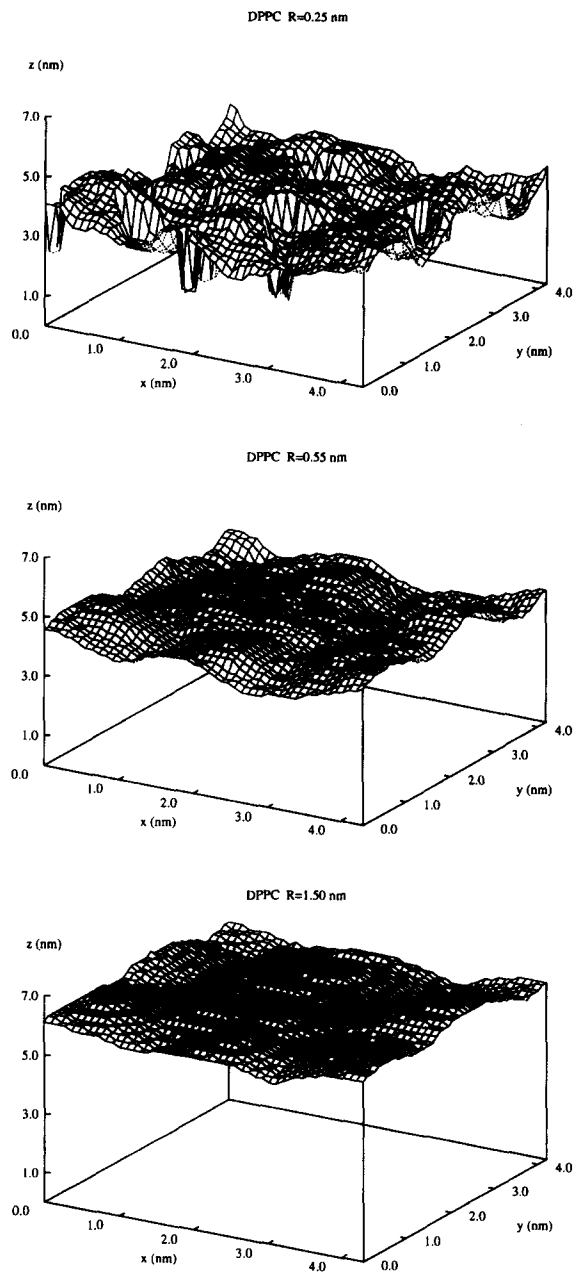

Fig. 4. The accessible surface for a probe with size 0.25, 0.55 and 1.50 nm for DPPC.

GLCB shows the difference in interfacial structure in that GLCB has more bulky head groups with more probe-accessible volume in between, compared to DPPC.

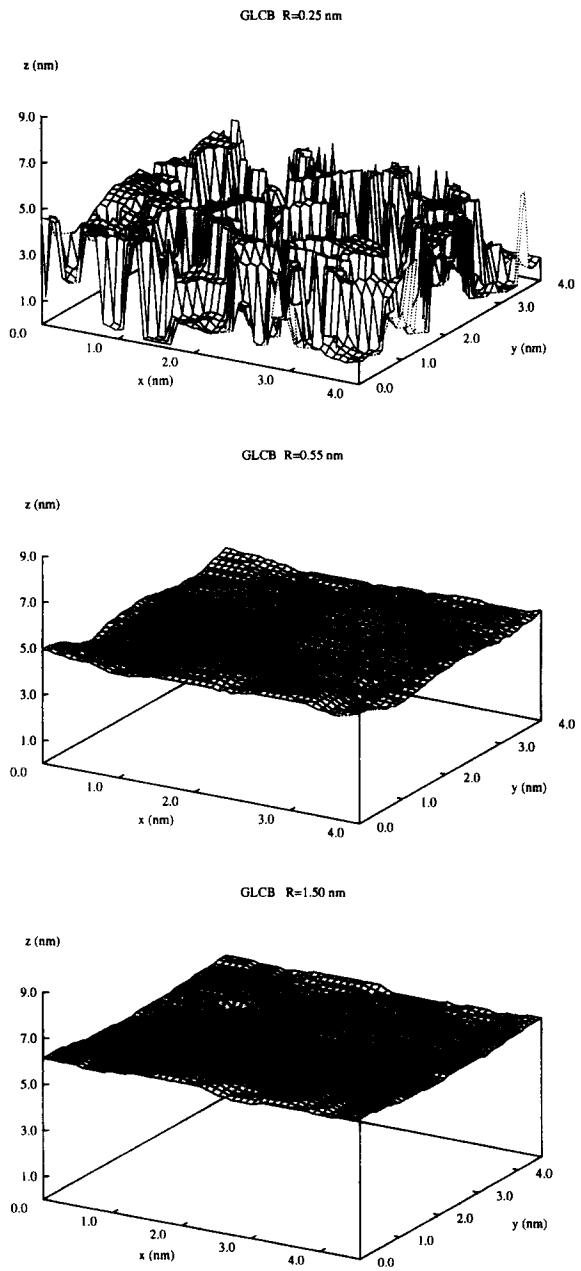

Fig. 5. The accessible surface for a probe with size 0.25, 0.55 and 1.50 nm for GLCB.

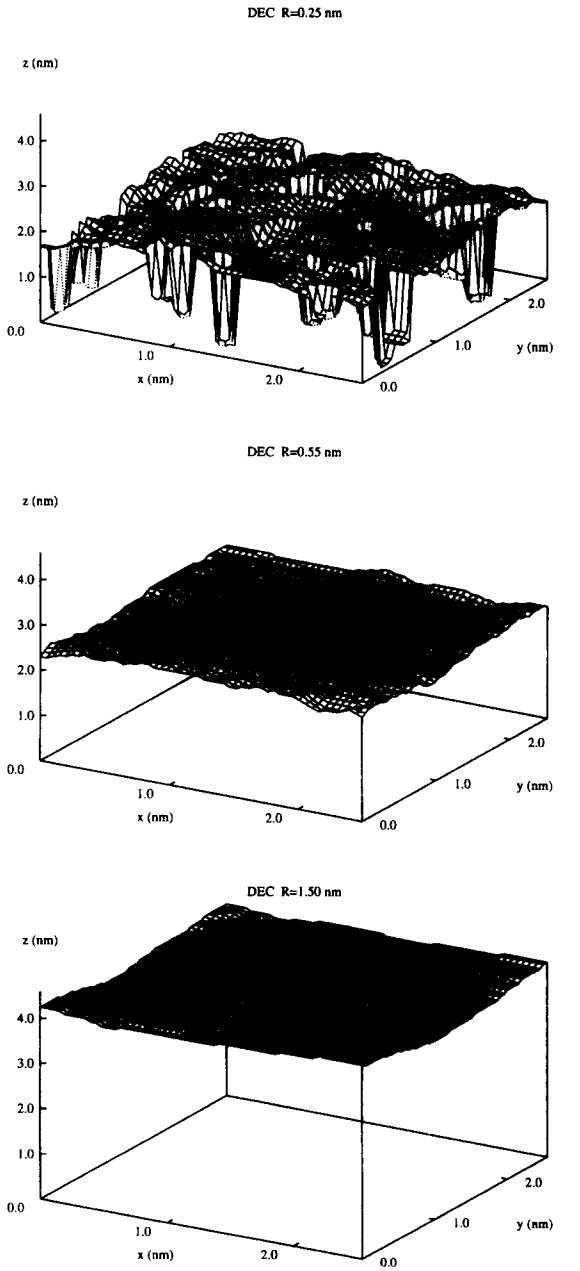

Fig. 6. The accessible surface for a probe with size 0.25, 0.55 and 1.50 nm for DEC.

Particle-accessible volume

In Fig. 8 we plot the accessible free volume for a probe with a size of 0.15 nm as a function of z-position in the box. From this figure it is clear that for a hydrophobic surface (DEC and GLYC) the accessible volume at the interface is higher than in both bulk phases. For a hydrophilic surface the opposite is observed; a decrease in free volume at

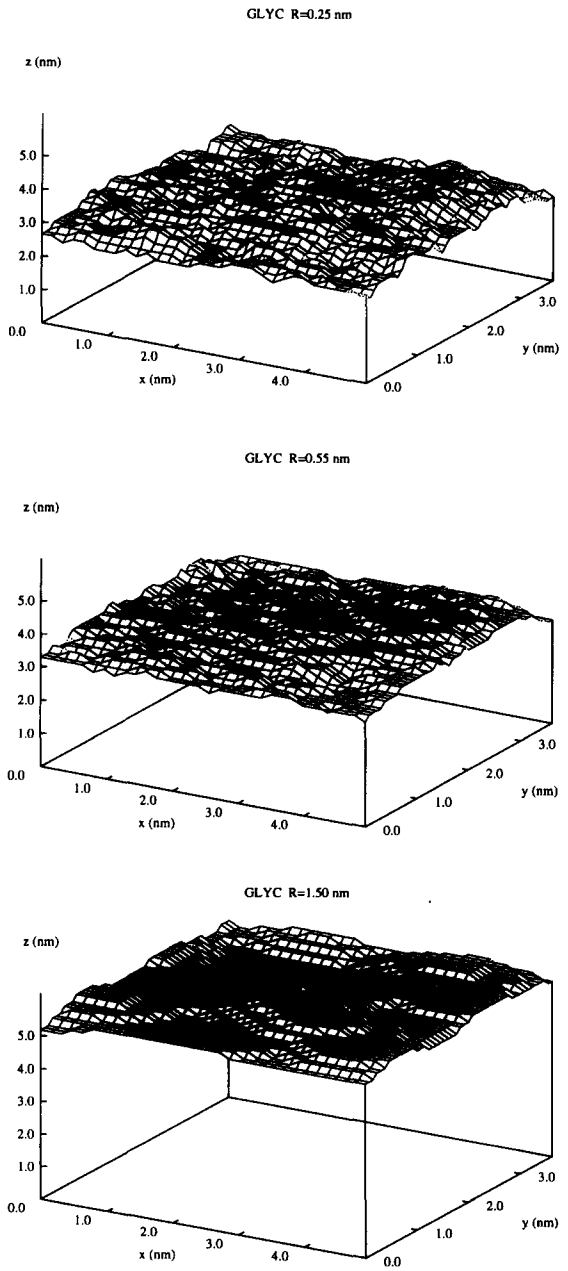

Fig. 7. The accessible surface for a probe with size 0.25, 0.55 and 1.50 nm for GLYC.

the interface. This effect was also observed by Pohorille and Wilson [21], and offers a nice way of distinguishing between hydrophobic and hydrophilic surfaces.

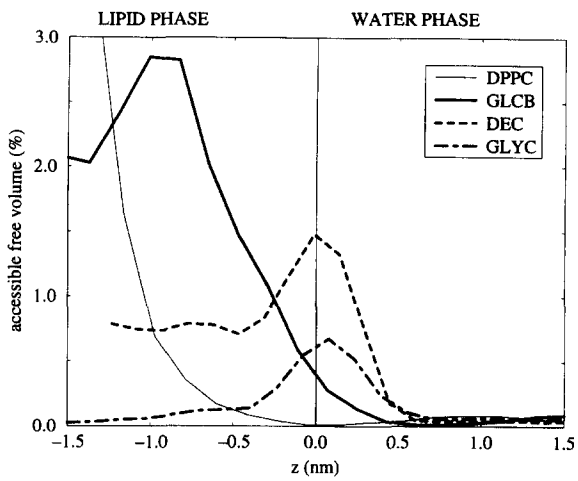

Fig. 8. The accessible volume (free volume) for a probe with size 0.15 nm as a function of z-position in the box for DPPC, GLCB, DEC and GLYC.

Electrostatic potential

Through the numerical evaluation of the double integral of the charge density ($\rho(z)$), the electrostatic potential (ψ) across the interface can be computed:

$$\psi(-\infty)-\psi(z)=-\int_{-\infty}^{z} dz' \int_{-\infty}^{z'} \rho(z'')dz''/\epsilon_0 \qquad (2)$$

where the position $z=-\infty$ is far enough in the bulk phase that the field is zero. By using this method, we are able to calculate the potential of the separate contributions, i.e., from the lipid, the water and the total potential. Computing the electrostatic potential in this way is consistent with the computed charge density using Poisson's equation, without the use of a cut-off radius. It is also possible to calculate the potential that is actually felt by the particles in the simulation (so including the cut-off), which is described in detail by Ahlström and Berendsen [11]. The separate contributions (lipid, water, and total) to the electrostatic potential are given in Fig. 9. The lipid potential builds up across the interface and is positive in the water phase for DPPC and GLCB. This is a result of the dipole orientation of the head groups, pointing towards the water phase. For GLYC the potential is slightly negative.

The water potential builds up negatively due to

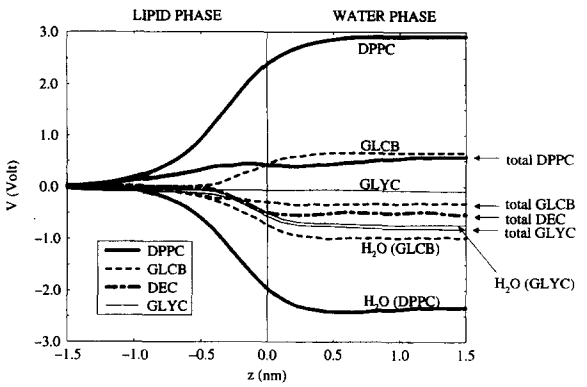

Fig. 9. Electrostatic potential across the interface against the z-position in the box. The interface is also plotted as defined in Fig. 2.

the preferential orientation of the water dipole towards the lipid phase as shown in Fig. 14. For the hydrophobic surfaces the water potential is only a result of the geometric constraints, because the decane molecules have no charge or dipole and the GLYC has only a very small dipole. For the hydrophilic surfaces, the water potential is primarily due to the compensation of the local dipolar charge distribution. A remarkable observation is that the cancellation of charges occurs throughout the entire interfacial region. Geometric constraints add a secondary effect, which even leads to a negative total potential difference across the interface for GLCB, i.e. an overcompensation of the lipid potential by the water molecules. The efficient compensation of a charge density by dipolar water orientation simply means that water acts as a medium with a high dielectric permittivity. This was also described for oleate/water bilayers [12].

We note however, that this holds for lipids that do have head groups with a dipole, but are uncharged. For charged lipids (dipalmitoylphosphatidylserine (DPPS) [20]) water is not able to fully compensate the lipid potential, which results in a total potential of a few volts. The potential difference across a monolayer has been measured experimentally and shows a more positive potential in the air (or oil) phase [35]. These measurements are not easy to perform. For example, for the water/air interface the experiments report a value of 0.025 V [36]. In our simulations, the total potential varies from slightly positive (DPPC, depending on the water layer thickness [14]) to slightly negative (GLCB, DEC, GLYC). So for the last three simulations this is in agreement with experiments on bilayers [37–39] and monolayers [35,40,41], at least for the sign. The value is overestimated, as was also observed for water/glycerol-1-monooleate [10] and water/DPPC/vacuum [11], although here the sign was positive. The latter is consistent with other DPPC results. According to Pohorille and Wilson [21] this may be dependent on the water model used and the lack of a polarization term in the potential function, neglecting the long-range forces and perhaps the system size. A reported compensation between dipolar and quadrupolar terms [21] does not play a role in our analysis: we computed the potential from the atomic charge distribution thus including all multipolar terms.

Electrostatics at the surface

When a particle approaches a surface from the aqueous side, it is not only influenced by the van der Waals surface as will be described in Section 3.2, but electrostatics plays a major role too. For example, the head group of a DPPC molecule can be thought of as a lever sticking into the water phase, and by moving, the electrostatics around this lever as felt by a particle approaching the interface changes drastically. The nitrogen group can stick into the water phase or into the hydrocarbon phase (as was observed in several simulations [14,16,42,43]) and therefore its position makes a large difference for the local potential. The same holds for the carbonyl groups and methyl groups, which are reported to contribute largely to the potential [40,41].

The local electrostatic potential (as opposed to the average potential described above) at a given point $\vec{r}$ in the aqueous phase is a complicated function of the position $\vec{r}_i$ and magnitude q_i of charges and of the dielectric susceptibility distribution. The water molecules shield the electric field and do this more effectively at larger distances from the interface. Since we only aim to give a qualitative picture of the potential distribution for snapshots of the simulation, we simply compute

the Coulombic potential $\psi(\vec{r})$ from

$$\psi(\vec{r}) = \frac{1}{4\pi\epsilon_0} \sum_i \frac{q_i}{|\vec{r}_i - \vec{r}|}, \quad (3)$$

summing over all partial charges in the system (using a grid), excluding solvent. We thus overestimate the potentials by a factor between 2 and 80, the higher factor applying to larger distances from the surface. It should also be noted that we only calculate the potential for one simulation box, as well as for one configuration. Therefore, at larger distances, the potential drops to zero, whereas a constant potential is reached for an infinite sheet of dipolar charges (see Fig. 9).

In Figs. 10, 11 and 12 the Coulombic potential is presented for DPPC, GLCB and GLYC (DEC is not charged). These plots are similar to the figures of the accessible surface from Section 3.1 in that the Coulombic potential is calculated at the positions 0.25, 0.55 and 1.50 nm from the defined interface (see Fig. 2). This is comparable to the probe sizes used for calculating the fractal dimension. Clearly the charge density is higher near the interface (0.25 nm) for all the three systems. Small white or black spots indicate the position of an atom that was positioned near or on a gridpoint. DPPC shows large areas of the same Coulombic potential due to larger charge groups, whereas GLCB and GLYC show more small areas of the same potential which correspond to the smaller hydroxyl and oxygen groups. For GLYC the potential at 1.50 nm is not given, because at this distance the potential is around zero. Also obvious from these plots is the higher (positive) Coulombic potential for DPPC with respect to GLCB and GLYC (note that the legend for DPPC runs from 0.50 to 1.0, whereas for GLCB and GLYC it runs from 0.35 to 0.65). This observation is in agreement with Fig. 9, where the DPPC contribution to the electrostatic potential was several volts (positive).

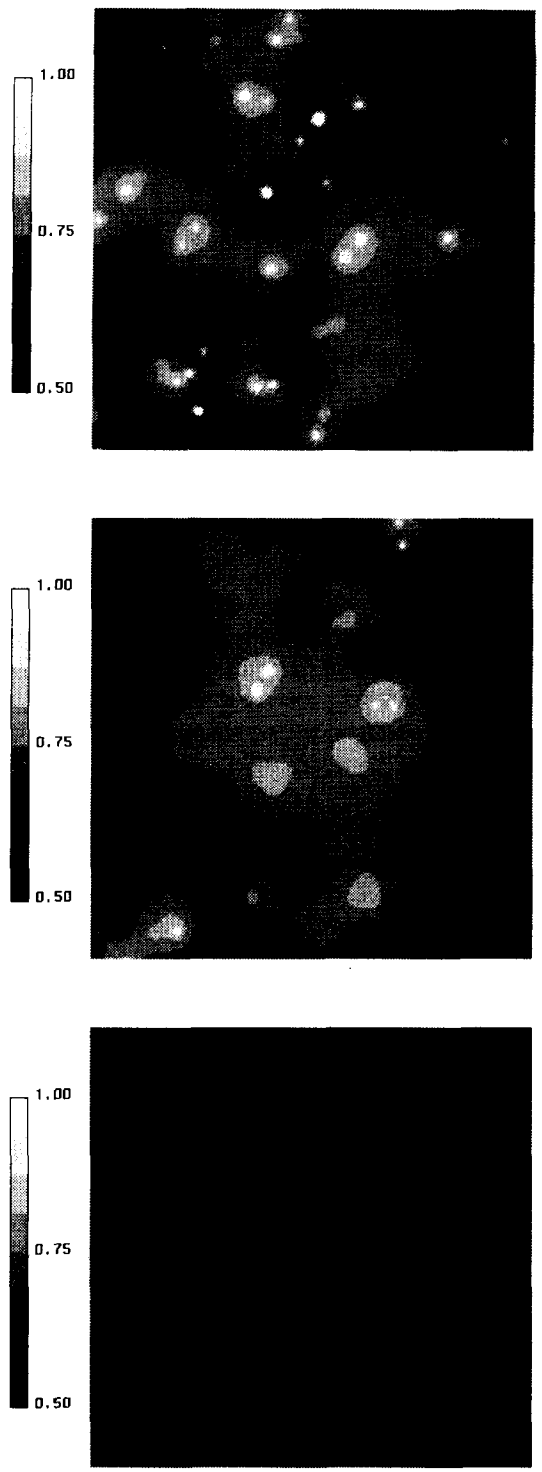

Fig. 10. The Coulombic potential at distance 0.25 (top), 0.55 (centre) and 1.50 nm (bottom) from the interface for DPPC. The range in the legend is from 0 to 7 V, where 0.50 equals zero potential. The x- and y-axes are the box lengths (nm) as given in Table 1.

3.2. Water

Hydrogen bonding

The properties of water are disturbed depending on the type of surface. A general aspect is that the water molecules close to the surface want to opti-

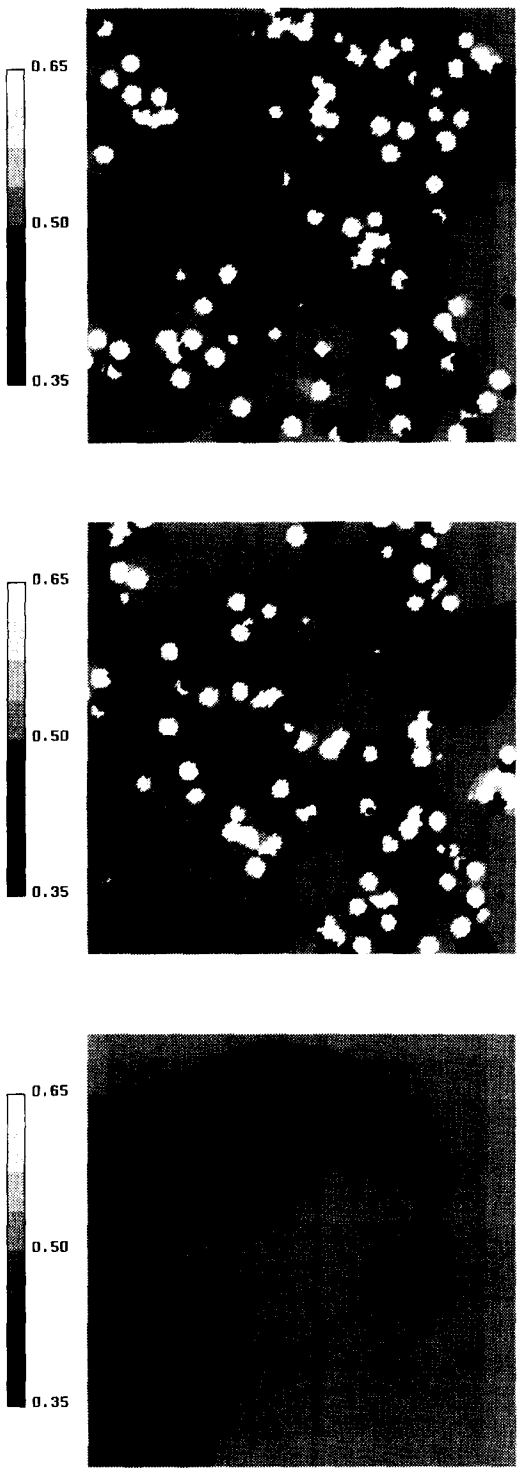

Fig. 11. The Coulombic potential at distance 0.25 (top), 0.55 (centre) and 1.50 nm (bottom) from the interface for GLCB. The range in the legend is from −2 to 2 V, where 0.50 equals zero potential. The x- and y-axes are the box lengths (nm) as given in Table 1.

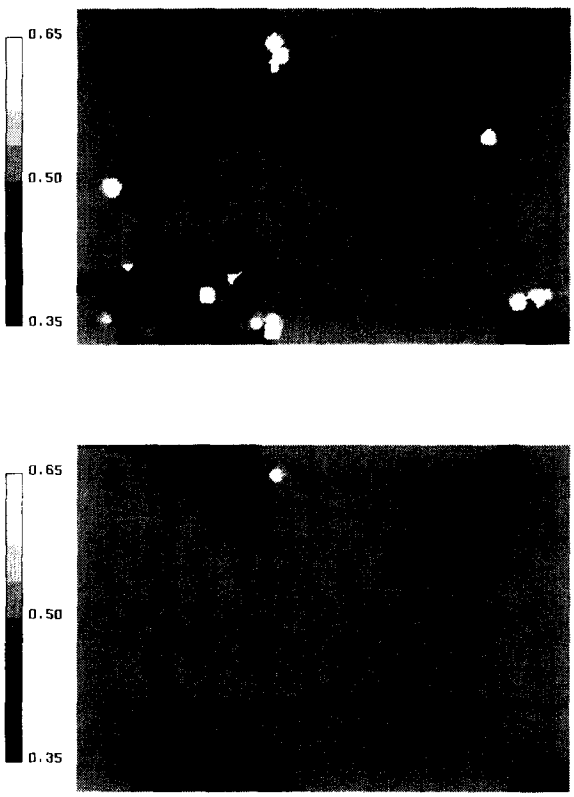

Fig. 12. The Coulombic potential at distance 0.25 (top) and 0.55 (centre) nm from the interface for GLYC. The range in the legend is from −2 to 2 V, where 0.50 equals zero potential. The x- and y-axes are the box lengths (nm) as given in Table 1.

mize their number of hydrogen bonds either with surrounding water molecules or with hydrogen-bonding groups at the interface. The possibility of forming hydrogen bonds with surrounding water molecules in bulk water is high. Therefore, the water molecules near the surface have to reorient themself to ensure an optimal number of hydrogen bond with surrounding molecules. For example, next to a flat surface the number of hydrogen bonds between the water molecules decreases, due to geometric constraints only [44,45]. The decrease is only about 25% however, instead of the

expected 50% for an unperturbed liquid. On average, the number of hydrogen bonds per water molecule decreases towards the interface, whereas the strength of the bonds increases [21]. For polar surfaces it was suggested that hydrogen bonding between water molecules decreases in the first layers of water, although the number of nearest neighbours to each water molecule increases [46]. This indicates that the electric fields near polar surfaces due to the surface charges, strongly orient water molecules. This was also observed by Egberts and co-workers [12,13] who found an almost complete cancellation of primary (ionic) surface charge density by water polarisation. This results in a weakening of the hydrogen-bond network.

By counting the number of water molecules within a sphere of 0.36 nm (which corresponds to the first minimum of the radial distribution function), we can obtain the number of nearest neighbours (NN) for a specific water molecule. The number of hydrogen bonds per water molecule with its surrounding water molecules was obtained by using a criterium of 10 kJ mol^{-1} as a cutoff for the pair energy. The ratio between the number of hydrogen bonds and the NN is a measure for the hydrogen-bonding structure between water molecules.

The hydrogen bonding between the water molecules from the bulk towards the interface is presented in Fig. 13. The lower figure represents the nearest neighbours (NN) and the number of hydrogen bonds of water with these neighbours, respectively. The upper figure gives the ratio of hydrogen bonds to NN. At the interface this ratio does not change so rapidly, which means that the interfacial water molecules have a preference to be bound to other water molecules, instead of to lipid molecules. The ability of making hydrogen bonds with other water molecules shows a clear increase towards the interface for all systems. For a flat surface, when only geometric constraints play a role, one would expect a value of $0.56 \times 0.75/0.5 = 0.84$. DEC approaches this value closest at the interface. Towards the bulk water phase the ratio rapidly decreases and levels off to a value around 0.56, which is comparable to the value of bulk SPC [47].

Although water–water hydrogen bonds are preferred, deficit hydrogen bonds are formed with head group atoms in the case of hydrophilic surfaces. This can be concluded from radial distribution functions (rdf's) between head group atoms and oxygen atoms of water molecules. The rdf's for DPPC and GLCB (data not shown here, but given in Refs. [9,14]) support the notion of strong hydrogen bonding of water with the head groups, and the presence of two to three peaks indicate multiple hydration shells. The partial charges on the head groups of DPPC account for the formation of large hydration shells, in which the water molecules are immobilized. This effect is less for GLCB and even lower for GLYC due to lower partial charges, but still profound.

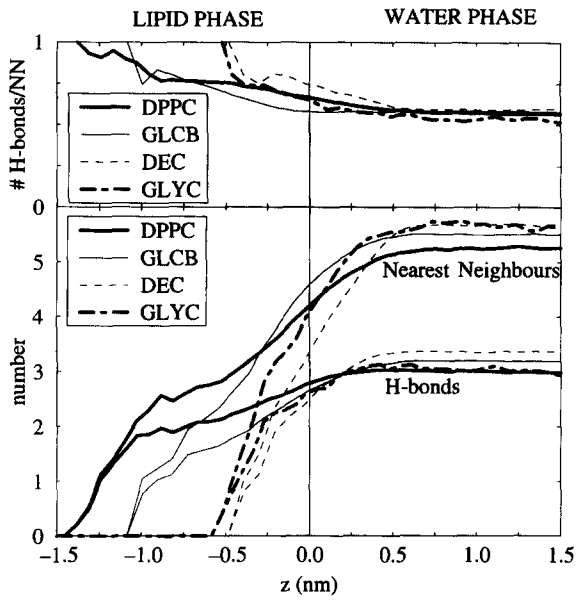

Fig. 13. Hydrogen bonds between neighbouring water molecules and number of nearest water neighbours as a function of distance to the interfacial plane. The upper figure gives the ratio of hydrogen bonds to NN.

Dipole orientation

The orientational order parameter of water-molecule dipoles is defined as the average cosine of the angle (θ_i) between the unit vector $\hat{\boldsymbol{\mu}}$ in the direction of the dipole, and the unit vector normal to the interface pointing outwards as seen from the water phase $\boldsymbol{n}_z$:

$$P_i(\theta) = \langle \cos \theta_i \rangle = \langle \hat{\boldsymbol{\mu}} \cdot \boldsymbol{n}_z \rangle. \quad (4)$$

In general, a water molecule at the interface has a preferential orientation of its dipole that lies parallel to the interface, i.e. one O–H bond pointing in the direction of and one away from the water phase. However, these orientational distributions are very broad and, moreover, asymmetric, which results in an excess dipole moment pointing away from the water phase. This observation is consistent in many simulations (see Refs. [7,8,11,13,17,18,21,45,48,49]).

The orientational order of the water molecules with respect to the interface expressed as the angle with respect to the interface is plotted in Fig. 14; the bigger this angle, the more the water dipole (and therefore the H-atom) orients towards the lipid layer. From this figure it is clear that the broad interface of DPPC influences the water molecules over a wide range. The stronger orientation of water is the result of the lipid dipolar potential. This effect of a severe orientation of the water dipole in the other simulations is not as profound and of a long range character, but definitely significant.

Another feature from Fig. 14 is that the ordering of the water molecules can be reversed: at the interface the dipole angle is positive, but at the aqueous side of the interface an opposite orientation is observed. This was also observed for the water/vapour interface [45,48,50,51]. For DPPC this effect is not clear, because it is drowned in the phospholipid-induced polarization. For GLCB, which is complicated by dipole orientation of the polar head groups, this effect is also not clear.

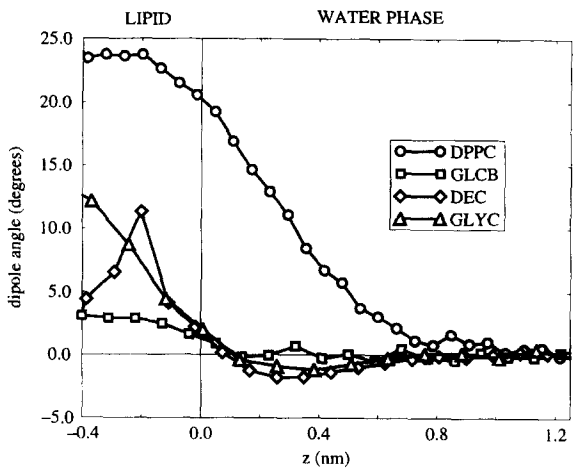

Fig. 14. Dipole angle of the water molecules as a function z-position in the box. The interface is also plotted as defined in Fig. 2.

Mobility

Diffusion rates of water molecules can be computed from their mean square displacement. The calculations of these diffusion rates are not very accurate due to noise as explained in Ref. [14], but are merely a qualitative indication. For hydrophilic surfaces the diffusion rates of water molecules near the interface are lower than in the (bulk) water phase see Refs. [8,12,14,17,20] due to hydrogen bonding of water molecules to head groups. These diffusion rates are in the order of 4.0×10^{-5} cm^2 s^{-1} at the interface and 8.0×10^{-5} cm^2 s^{-1} in bulk water for the DPPC/water interface at 350 K [14]. For hydrophobic surfaces such as GLYC, the difference between diffusion rates remains within the noise [6].

3.3. Lipids

Order parameters of the tails

For the orientational preference of the alkyl tails we calculated the order parameters of a designated molecular axis with respect to the simulation box:

$$S = \tfrac{3}{2}\langle \cos^2 \theta \rangle - \tfrac{1}{2}, \qquad (5)$$

where θ is the angle between the z-axis of the simulation box and the molecular axis under consideration. Brackets imply averaging over time and molecules.

In Fig. 15 the order parameters per CH_2 segment of the alkyl tails are presented. The molecular axis at C_n is defined as the vector from C_{n-1} to C_{n+1}. The tails of DPPC and GLCB show an overall orientation that is perpendicular to the interface, with the notion that towards the end of the tails the order becomes lower. The plot for DPPC shows two values at the position of carbon number 2, as the data between the two tails are significantly different. The data are in good agreement with experiment as was discussed in Ref. [13]. For GLCB the oxygen attached to the glucose head group is also plotted, to stress the importance of

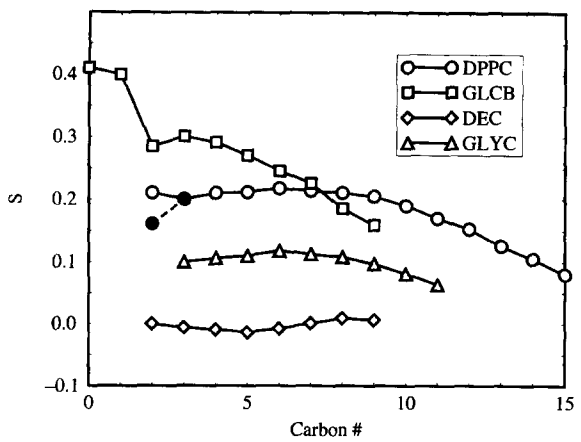

Fig. 15. Order parameters per CH_2 segment of the alkyl tails. For DPPC and GLYC the data of both tails is shown in one plot.

how the head group is presented towards the oil phase [9]. Although the GLYC simulation is an interface between (bulk) oil and (bulk) water, the alkyl tails of GLYC show a significant ordering in the bulk oil phase on the whole. This aspect is discussed in more detail in Ref. [6]. For DEC an overall isotropic orientation is observed, as is to be expected for a liquid oil phase.

The order parameter as a function of z-position in the box was evaluated as well, but only shown for GLYC and DEC in Fig. 16, to show the ordering of oil molecules in contact with water. The results of these plots indicate that the oil molecules orient themselves laterally ($S<0$) towards the interface to ensure that the total hydrophobic surface in contact with water is as small as possible.

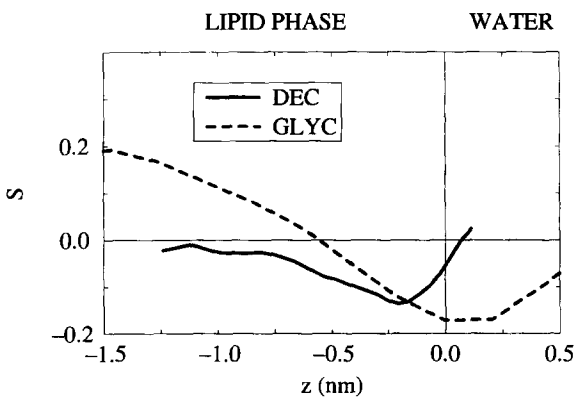

Fig. 16. Order parameter of the CH_2 segments of the alkyl tails as a function of distance z to the interface.

Mobility

From the slope of the mean square displacement (MSD) curve of particles versus time the apparent diffusion constant D can be evaluated:

$$D = \lim_{t-\infty} \frac{1}{2dt} \langle [r(t)-r(0)]^2 \rangle, \quad (6)$$

where $r(t)$ stands for the position vector of a particle at time t, and the brackets denote an ensemble average. The number of dimensions is given by the factor d: $d=1$ for linear, $d=2$ for lateral, and $d=3$ for bulk diffusion.

The diffusion of lipids is a slow process and is in the order of 10^{-7} to 10^{-8} $cm^2\ s^{-1}$. Our simulation times for DPPC and GLCB are not long enough to calculate long time diffusion constants accurately. Therefore, short time diffusion within 10 ps is used as a measure for the mobility of the interface. This is in fact characteristic for the motion of lipids in their local potential wells, or sometimes referred to as "rattling in their cage". From Table 2 it is clear that the lipids in the hydrophilic surfaces are not very mobile and that the head groups of DPPC and GLCB are more mobile than the lipids as a whole. Owing to decreased lipid–lipid interactions at the hydrophobic surfaces, the mobilities of these lipids are expected to be much higher, although this is not obvious from Table 2.

Video animations of the trajectories [31,32] are also very informative on the dynamical behaviour

Table 2
Apparent diffusion constants, short and long time, per lipid as a whole and for the head groups

System	D_{lipid} ($cm^2\ s^{-1}$)	D_{head} ($cm^2\ s^{-1}$)
Short time diffusion		
DPPC	$6(\pm 1)\times 10^{-6}$	$10(\pm 1)\times 10^{-6}$
GLCB	$3(\pm 1)\times 10^{-6}$	$7(\pm 1)\times 10^{-6}$
DEC	$6(\pm 1)\times 10^{-6}$	–
GLYC	$6(\pm 1)\times 10^{-6}$	–
Long time diffusion		
DEC	$2(\pm 0.1)\times 10^{-6}$	–
GLYC	$1(\pm 0.1)\times 10^{-6}$	–

of the lipids and the head groups, and showed very flexible, diffuse lipid layers within the simulation time. We did not observe lipid molecules completely dissolve into the water phase, owing to longer time scales of such a process. Protruding motions of the lipid molecules were observed however, up to several carbon atoms of the alkyl tails in contact with the water phase.

4. Conclusion

For a number of simulated surfaces ranging from completely hydrophobic to hydrophilic, with water as one of the bulk phases, we have analyzed various surface properties with respect to the roughness, mobility, hydrophobicity and surface charge distribution and potential. Also the structural ordering of water and lipid phase has been considered.

Although the simulations concern widely varying hydrophobic and amphiphilic components and cover a range of temperatures, the various surface structure show very similar properties. The salient points are summarized below.

4.1. Roughness

All simulated surfaces between water and liquid or liquid-crystalline phases have a similar appearance: the interfacial width is appreciable, varying between 0.5 nm for liquid interfaces and 1 nm for interfaces containing surfactant molecules. The more hydrophilic the non-aqueous interface, the rougher its surface is. None of the interfaces are sharp on a molecular scale. They all have a rough, fractal surface as seen by particles of atomic size (0.2 to 0.5 nm), but become smooth, planar surfaces on the nm scale.

4.2. Mobility

A hierarchy of dynamic time scales exists for various aspects of the surface:

(a) Internal alkane chain mobility (trans–gauche isomerism) occurs on a 10 ps time scale. Exceptions are conformational states of lecithins (two conformers of the *SN*2 chain) which have macroscopic life times (seconds).

(b) Perpendicular motions of individual molecules occur on a time scale of several tens of picoseconds. These include temporary partial dissolution of amphiphatic molecules over a few atoms length.

(c) Lateral motions of atomic size also occur on a time scale of several tens of picoseconds.

(d) Lateral motions of a diffusional character can be observed on a nanosecond time scale.

(e) Complete dissolution of amphiphiles in water does not occur in our simulation times. Neither do molecular flips between bilayer leaflets occur.

Water diffuses almost as in the bulk phase: both translational and rotational diffusion is slowed down in the interface region by a factor of 2 to 3 at most, near hydrophilic surfaces.

4.3. Surface potential

Computer simulations give detailed insight into the charge distribution and resulting electrical potential across interfaces. The most striking result, observed in several different simulations, is the almost complete compensation of the primary charge distribution, due to charge or dipoles of molecules at the interface, by polarization of water. The average orientation of water molecules adjusts itself in the local field such that a compensating charge distribution results. In fact this means that water behaves as an ideal dielectric medium, even in regions of the interface where the water density is low. It can fulfill this role because the surface layer is diffuse; a sharp boundary would act more as a traditional double layer with its electrical potential extending into the aqueous phase. The charged lipid DPPS [20] behaves more like a charged double layer with resulting net electric potential difference over the interface. The electrical field in our simulations does not extend much further than the thickness of the surface layer itself. The "dielectric constant" looses its meaning at the interface, as the charge compensation involves not only dipolar terms, but also higher moments. Only the charge density to the divergence of the dipole moment density is related in the dielectric constant. Apart from the — generally dominant — water polarization in response to primary charges and dipoles, water exhibits a slight preferential orienta-

tion with its dipole directed outwards from the water phase. This is the cause of an intrinsic potential difference over a hydrophobic interface. This intrinsic tendency may in some cases even cause an overcompensation of the primary charge density, thus reversing the expected interface potential.

The interfaces show a different behaviour at a microscopic level. We can conclude from our study that the interfaces are in a "local" minimum and are stable. Although lateral movement does not occur within shorter simulation times, due to protrusions and head group movement, the interface will adjust itself relatively fast (tens of picoseconds). When for example a protein diffuses towards the interface, we expect the lipids to adjust locally very rapidly enabling the protein to bind, where the protein adjusts itself (rotation, deformation) on a much longer timescale. The protein therefore, is the limiting factor in membrane–protein binding processes.

Acknowledgement

This research was supported in part by Unilever Research Laboratory (URL), Vlaardingen, the Netherlands, and in part by the Foundation for Biophysics with financed aid from the Netherlands Research Organisation.

References

[1] W.F. van Gunsteren and A.E. Mark, Eur. J. Biochem., 204 (1992) 947–961.
[2] M.P. Allen and D.J. Tildesley, Computer Simulations of Liquids, Clarendon, Oxford, 1987.
[3] W.F. van Gunsteren and H.J.C. Berendsen, Angew. Chem. Int. Ed. Engl., 29 (1990) 992–1023.
[4] I.L. Carpenter and W.J. Hehre, J. Phys. Chem., 94 (1990) 531–536.
[5] A.R. van Buuren, S.J. Marrink and H.J.C. Berendsen, J. Phys. Chem., 97 (1993) 9206–9212.
[6] A.R. van Buuren, J. de Vlieg and H.J.C. Berendsen, Langmuir, in press.
[7] J. Gao and W.L. Jorgensen, J. Phys. Chem., 92 (1988) 5813–5822.
[8] I. Benjamin, J. Chem. Phys., 97 (1992) 1432–1445.
[9] A.R. van Buuren and H.J.C. Berendsen, Langmuir, 10 (1994) 1703–1713.
[10] M.A. Wilson and A. Pohorille, J. Am. Chem. Soc., 116 (1994) 1490–1501.
[11] P. Ahlström and H.J.C. Berendsen, J. Phys. Chem., 97 (1993) 13691–13702.
[12] E. Egberts and H.J.C. Berendsen, J. Chem. Phys., 89 (1988) 3718–3732.
[13] E. Egberts, S.J. Marrink and H.J.C. Berendsen, Eur. Biophys. J., 22 (1994) 423–436.
[14] S.J. Marrink, M. Berkowitz and H.J.C. Berendsen, Langmuir, 9 (1993) 3122–3131.
[15] S.J. Marrink and H.J.C. Berendsen, J. Phys. Chem., 98 (1994) 4155–4168.
[16] T.R. Stouch, Molec. Simulations, 10 (1993) 335–362.
[17] H.E. Alper, D. Bassolino-Klimas and T.E. Stouch, J. Chem. Phys., 99 (1993) 5547–5559.
[18] K.V. Damadoran, and K.M. Merz Jr. Langmuir, 9 (1993) 1179–1183.
[19] K. Raghavan, M.R. Reddy and M.L. Berkowitz, Langmuir, 8 (1992) 233–240.
[20] J. Lopez Cascales, J. Garcia de la Torre, S.J. Marrink and H.J.C. Berendsen, Eur. Biophys. J., in press.
[21] A. Pohorille and M.A. Wilson, J. Mol. Struc., 284 (1993) 271–298.
[22] P. van der Ploeg and H.J.C. Berendsen, J. Chem. Phys., 76 (1982) 3271–3276. It should be noted that there is a significant typographic error in the paper. For both methylene and methyl σ should be $\sigma = 0.374$ nm.
[23] P. van der Ploeg, H.J.C. Berendsen, Molec. Phys., 49 (1983) 233–248.
[24] B. Smit, P.A.J. Hilbers, K. Esselink, L.A.M. Rupert, N.M. van Os and A.G. Schlijper, Nature, 348 (1990) 624–625.
[25] B. Smit, A.G. Schlijper, L.A.M. Rupert and N.M. van Os, J. Phys. Chem., 94 (1990) 6934.
[26] S. Karaborni, S. Toxvaerd and O.H. Olsen, J. Phys. Chem., 96 (1992) 4965–4973.
[27] J. Harris and S.A. Rice, J. Chem. Phys., 89 (1988) 5898–5908.
[28] W.F. van Gunsteren and H.J.C. Berendsen, Gromos-87 manual. Biomos BV, Nijenborgh 4, 9747 AG Groningen, The Netherlands.
[29] H.J.C. Berendsen, J.P.M. Postma, W.F. Gunsteren and J. Hermans, Intermolecular Forces. B. Pullman, Reidel Dordrecht, Holland, (1981).
[30] D. van der Spoel, H.J.C. Berendsen, A.R. van Buuren, E. Apol, P.J. Meulenhoff, A.L.T.M. Sijbers and R. van Drunen, Gromacs user manual. Biomos BV, Nijenborgh 4, 9747 AG Groningen, The Netherlands.
[31] S.J. Marrink and H.J.C. Berendsen, Video: the real face of membranes (1993). A copy of this video (VHS, PAL or NTSC) can be obtained for US$40, BIOMOS bv. Nijenborgh 4, 9747 AG Groningen, The Netherlands.
[32] A.R. van Buuren and H.J.C. Berendsen, Video: Monolayer surfactant dynamics (1994). A copy of this video (VHS, PAL or NTSC) can be obtained for US$40, BIOMOS bv. Nijenborgh 4, 9747 AG Groningen, The Netherlands.

[33] P. Pfeifer and D. Avnir, J. Chem. Phys., 79 (1983) 3558–3565.
[34] M. Lewis and D.C. Rees, Science, 230 (1985) 1163–1165.
[35] C.M. Knobler, Adv. Chem. Phys., 77 (1990) 397–449.
[36] J.R. Farrell and P. McTigue, J. Electroanal. Chem., 139 (1982) 37–56.
[37] R.F. Flewelling and W.L. Hubbell, Biophys. J., 49 (1986) 541–552.
[38] K. Gawrisch, D. Ruston, J. Zimmerberg, V.A. Parsegian, R.P. Rand and N. Fuller, Biophys. J., 61 (1992) 1213–1223.
[39] S.A. Simon and T.J. McIntosh, Proc. Natl. Acad. Sci. USA, 86 (1989) 9263–9267.
[40] V. Vogel and D. Möbius, Thin Solid Films, 159 (1988) 73–81.
[41] ????
[42] H. Heller, M Schaefer and K. Schulten, J. Phys. Chem., 97 (1993) 8343–8360.
[43] D. Stigter and K.A. Dill, Langmuir, 4 (1988) 200–209.
[44] C.Y. Lee, J.A. McCammon and P.J. Rossky, J. Chem. Phys., 80 (1984) 4448.
[45] M. Matsumoto and Y. Kataoka, J. Chem. Phys., 88 (1988) 3233–3245.
[46] R. Kjellander and S. Marcelja, Chem. Phys. Lett., 120 (1985) 393.
[47] J.P.M. Postma, A Molecular Dynamics Study of Water. PhD thesis, University of Groningen, The Netherlands (1985).
[48] M.A. Wilson, A. Pohorille and L.R. Pratt, J. Phys. Chem., 91 (1987) 4873.
[49] R. Kjellander and S. Marcelja, Chemica Scripta, 25 (1985) 73–80.
[50] M.A. Wilson, A. Pohorille and L.R. Pratt, J. Chem. Phys., 88 (1988) 3281–3285.
[51] S. Tsunashima, H.E. Gunning and O.P. Strausz, J. Am. Chem. Soc., 98 (1976) 1690.